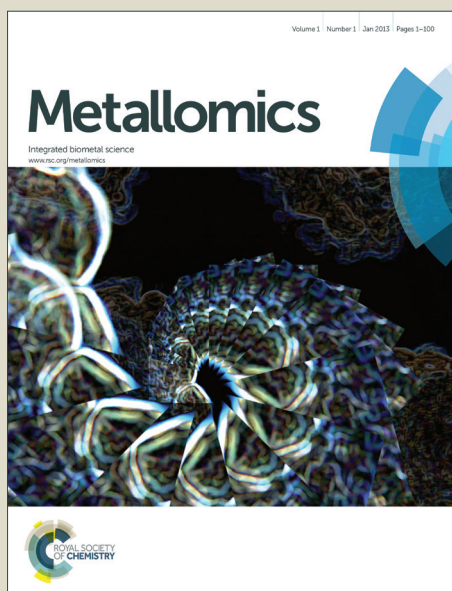


Metallomics

Accepted Manuscript



This is an *Accepted Manuscript*, which has been through the Royal Society of Chemistry peer review process and has been accepted for publication.

Accepted Manuscripts are published online shortly after acceptance, before technical editing, formatting and proof reading. Using this free service, authors can make their results available to the community, in citable form, before we publish the edited article. We will replace this *Accepted Manuscript* with the edited and formatted *Advance Article* as soon as it is available.

You can find more information about *Accepted Manuscripts* in the [Information for Authors](#).

Please note that technical editing may introduce minor changes to the text and/or graphics, which may alter content. The journal's standard [Terms & Conditions](#) and the [Ethical guidelines](#) still apply. In no event shall the Royal Society of Chemistry be held responsible for any errors or omissions in this *Accepted Manuscript* or any consequences arising from the use of any information it contains.

1
2
3 **Metal ion mediated transition from random coil to β -sheet and aggregation of Bri2-23, a**
4
5 **natural inhibitor of A β aggregation.**
6
7
8
9

10
11 Marek Luczkowski,^{†*} Riccardo De Ricco,[‡] Monika Stachura,[§] Slawomir Potocki,[†] Lars
12
13 Hemmingsen,[§] Daniela Valensin^{‡*}
14

15
16 [†]*Faculty of Chemistry, University of Wroclaw, F. Joliot Curie 14, 50-383 Wroclaw, Poland*
17

18
19 [‡]*Department of Biotechnology Chemistry and Pharmacy University of Siena, Via A. Moro*
20
21 *53100 Siena, Italy*
22

23
24 [§]*Department of Chemistry, University of Copenhagen, Universitetsparken 5, 2100*
25
26 *Copenhagen, Denmark*
27

28
29
30
31
32
33 * e-mail: marek.luczkowski@chem.uni.wroc.pl, daniela.valensin@unisi.it
34
35
36
37
38
39
40
41
42
43
44
45
46
47
48
49
50
51
52
53
54
55
56
57
58
59
60

Abstract

Furin-dependent maturation of the BRI2 protein generates the BRI2-23 fragment that is able to arrest the aggregation of amyloid β , the peptide implicated in Alzheimer's disease (AD). BRI2-23 contains cysteines at positions 5 and 22 which are likely to bind to metal ions such as Cu(I). Metal ions may play a role in the etiology of neurodegenerative disorders such as AD, and in this work we explore the metal ion induced folding and aggregation of BRI2-23 using Hg(II) and Ag(I) as spectroscopic probes with structural and ligand preferences similar to those of Cu(I), while not displaying redox activity under the experimental conditions. In general, interaction of BRI2-23 with soft metal ions changes structural properties and solution behavior of the peptide that tune to increasing metal to peptide stoichiometry. Potentiometric, $^{199\text{m}}\text{PAC}$ and ESI-MS data indicate that addition of up to 0.5 equivalents of Hg(II) to BRI2-23 yields two-coordinated HgS_2 structure at the metal site. While free peptide is inherently unstructured, the presence of Ag(I) and Hg(II) gives rise to β -sheet formation. NMR spectroscopy supports the formation of β -sheet structure in the presence of 0.5 equivalents of Hg(II), and displays an interesting and marked change in the TOCSY spectra when increasing the Hg(II) to peptide stoichiometry from 0.5 to 0.7 equivalents, indicating the equilibrium between two structural analogues of the complex. Addition of more than 0.7 equivalents of Hg(II) give rise to line broadening, presumably reflecting aggregation. This is further supported by ThT fluorescence studies showing that BRI2-23 peptide does not aggregate over 24 hours, while addition of over 0.7 equivalent of Ag(I) or Hg(II) leads to increase of fluorescence, indicating that these metal ions induce aggregation. Thus, a model integrating all data into a coherent picture is that metal ion binding to the two thiolates gives rise to folding of the peptide into a structure that is prone to aggregation, forming aggregates with a considerable amount of β -sheet. Molecular dynamics simulations initiated with structures that agree with NMR data additionally support this model.

Keywords: BRI2, aggregation inhibitor, probe, Cu(I), Hg(II), A β .

Introduction

BRI2, also known as *ITM2b*, is a type II transmembrane protein of unknown function abundantly expressed in neuronal tissues. It is 266 amino acids long and can be divided into a large C-terminal extracellular domain, a transmembrane domain, and a short N-terminal cytoplasmic domain. Mutations of the *ITM2b* gene result in expression of the protein precursors ABriPP and ADanPP.¹ Like the amyloid precursor protein (APP), BRI2 is subject to enzymatic processing by a number of proteolytic enzymes, including prohormone furin-like convertases able to cleave the WT BRI2 protein near the C-terminus to produce a 23-amino acid peptide, called BRI2-23 (Figure 1). Similarly to WT BRI2, also ABriPP and ADanPP proteins undergo to proteolytic cleavage at the C-terminal region generating ABri and ADan peptides (Figure 1).^{2,3} These peptides constitute the hallmarks of the Familiar British Dementia (FBD) and Familiar Danish Dementia (FDD) disorders, that share many mechanistic and pathological similarities with Alzheimer's disease (AD).¹ This process is initialized by the activation of the convertase in *trans* region of the Golgi apparatus and continues once the secretory vesicle merges with the cellular membrane. Although both the Golgi lumen and extracellular space represent the exoplasmic face of the membrane, they differ in redox potential, with the lumen being more reductive environment.^{4,5}

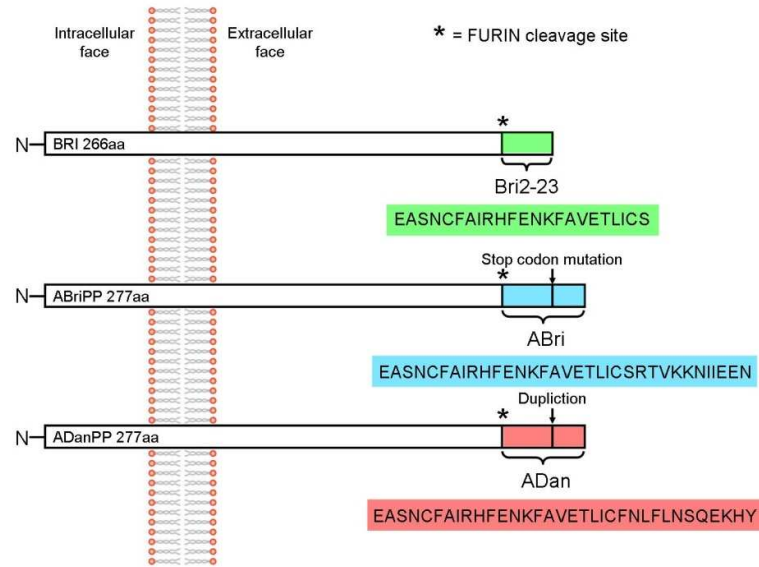


Figure 1. Schematic representation of BRI2 protein, its disease related forms and the products of their enzymatic processing by furin.

The accumulation of ABri and ADan triggers a complex pathological cascade of events leading to neurodegeneration,^{6,7} while BRI2-23 preserves its solubility.⁸ Both ABri and ADan peptides exist in reduced or oxidized form due to the presence of two cysteine residues within the peptide sequence, which are able to form disulphide bridges.⁹ However, the consequences of the oxidation are found to be contradictory with respect to the peptides' susceptibility to form oligomers and to aggregate.¹⁰ While intramolecular disulphide bridge promotes the β sheet formation and aggregation with subsequent fibrillation in ABri,¹¹ the amyloid-like aggregates of ADan are mainly formed by the reduced form of peptide.¹⁰ These contradictory results imply that the upstream formation of non-fibrillar soluble oligomers rather than insoluble aggregates represent the pathogenic species cause neurodegeneration.^{10,}

12

Contrary to the ABri and ADan behavior, the wild type peptide, BRI2-23 has no toxic effects, yielding neither oligomers nor aggregates of high order. Interestingly, BRI2-23 has been found to inhibit A β aggregation *in vitro* and *in vivo*.¹³ This inhibitory effect is probably

1
2
3 mediated by the fragment containing –FENKF– sequence, that is analogous to that found in
4
5 peptidic inhibitors of amyloid aggregation (–KLVFF–).¹⁴ Moreover, a peptide encompassing
6
7 similar sequence has been demonstrated to interact with the glycine-zipper segment of A β 1-40
8
9 (–G₃₃XXXG₃₇–) that is critical for the formation of stable β sheet structure.^{14,15} In addition, the
10
11 BRI2-23 peptide transported to the plasma membrane, is able to interact with APP reducing
12
13 the access of α -, β - and γ -secretases to their respective cleavage sites.¹⁶ As a result, the release
14
15 of any APP metabolite, including A β , is reduced.
16
17

18
19 Transition metal ions, like Cu, Zn and Fe are implicated in many neurodegenerative
20
21 disorders and are believed to influence either the aggregation of amyloidogenic proteins or the
22
23 formation of reactive oxygen species (ROS).¹⁷⁻²⁸ Metal ions are involved in the aggregation of
24
25 ABri and ADan peptides as well.²⁰ On the other hand nothing is known about the metal binding
26
27 abilities of BRI2-23 and more important whether metal ions affect its structure and
28
29 aggregation ability. BRI2-23 contains several residues, like Cys, His, Glu (Figure 1) which
30
31 might interact with metal transition ions. In particular, the presence of two cysteines points
32
33 out a possible Cu(I)-S₂ coordination geometry and high Cu(I)-BRI2-23 affinity.
34
35
36
37

38
39 Herein, we aim at investigating the interaction between Cu(I) and BRI2-23 by
40
41 combining experimental and theoretical methods. In order to elucidate the role, if any, played
42
43 by the cuprous ion we used Hg(II) or Ag(I), as spectroscopic probes of Cu(I),²⁹ while
44
45 Molecular Dynamics calculations (MD) were performed by using Cu(I). The choice to use
46
47 Hg(II) and Ag(I) as Cu(I) probes, was due to the fact that Cu(I) is a redox active metal which
48
49 can easily oxidize to Cu(II). For this reason sample preparation is usually performed in inert
50
51 atmosphere and in presence of reducing agents such as ascorbic acid or dithionite.
52
53 Unfortunately, such procedure does not completely exclude the presence of Cu(II), which
54
55 although very small can interfere with Cu(I)-BRI2-23 binding in two different ways: (i) by
56
57 interacting with the peptide and by oxidizing Cys residues. Moreover, Hg(II) and Ag(I) ions
58
59
60

1
2
3 are commonly used to investigate Cu(I) sites, as demonstrated by previous studies.³⁰⁻⁴¹ By
4
5 applying a multi techniques approach we characterize the metal coordination sphere, the
6
7 binding affinity and stoichiometry, the speciation profiles and the structural rearrangements of
8
9 BRI2-23 induced by the metal ion.
10

11 12 13 14 15 16 **Experimental section**

17 18 *Peptide Synthesis and Purification*

19
20 Peptides were synthesized on an Activotec Activo-P11 automated peptide synthesizer,
21
22 on 0.25 mmol scale using standard Fmoc chemistry.⁴² Fmoc-Ser(tBu)-Wang resin was used
23
24 as the solid support so that the resulting peptides would have unprotected C-terminus as in
25
26 natural system. Cleavage from the resin was performed for 120 min in a 90% trifluoroethanol
27
28 (TFA) solution containing 5% thioanisole, 2% anisole, and 3% ethanedithiol as free radical
29
30 scavengers. After precipitation with cold ether, the peptides were redissolved in water and
31
32 lyophilized to obtain a fluffy off-white powder. The solid was redissolved in 10% acetic acid
33
34 and purified by reversed phase HPLC on a Varian Prostar HPLC with a preparative C18
35
36 column (Varian Pursuit XRs C 18) with a semi-linear gradient of 0.1% TFA in water to 0.1%
37
38 TFA in 9:1 CH₃CN/H₂O over 45 min. The identity of the peptides was verified by ESI
39
40 (electrospray ionization) mass spectrometry.
41
42
43
44
45

46 47 *ThT fluorescence spectroscopy assay*

48
49 The fluorometric assay was performed on FP-6500 JASCO spectrofluorometer. The
50
51 peptide Bri2-23 was analyzed in presence and in absence of 0.7 equivalents of Ag(I) and
52
53 Hg(II). 50 mM phosphate buffer solutions were used to dissolve the peptide to a final
54
55 concentration of 10 μM. Thioflavin-T was added to all analyzed systems to give a 10 μM final
56
57
58
59
60

1
2
3 concentration. All the samples were monitored immediately after the preparation and after one
4
5 day of incubation at room temperature.
6

7 8 *Mass spectrometry* 9

10
11 High-resolution mass spectra were obtained on a BrukerQ-FTMS spectrometer
12
13 equipped with an Apollo II electrospray ionization source with an ion funnel. The mass
14
15 spectrometer was operated in the positive ion mode with the following parameters: scan range
16
17 m/z 400–1600, dry gas-nitrogen, temperature 170°C, ion energy 5 eV. Capillary voltage was
18
19 optimized to 4500 V to obtain the highest S/N ratio. Changing the voltage (± 500 V) did not
20
21 significantly affect the optimized spectra. The samples (metal/ligand in a 1:1 stoichiometry,
22
23 $c_{\text{BR12-23}} = 1 \times 10^{-4} \text{M}$) were prepared in 9:9:2 MeOH/H₂O/DMSO mixture in carbonate buffer
24
25 pH 6.5. Variation of the solvent composition down to 5% of MeOH did not change the
26
27 speciation. The sample was infused at a flow-rate of 3 mLxmin⁻¹. The instrument was
28
29 calibrated externally with the Tunemix™ mixture (Bruker Daltonik, Germany) in quadratic
30
31 regression mode. Data were processed by using the Bruker Compass Data Analysis 4.0
32
33 program. The mass accuracy for the calibration was higher than 5 ppm, enabling together with
34
35 the true isotopic pattern (SigmaFit) an unambiguous confirmation of the elemental
36
37 composition of the obtained complex.
38
39
40
41

42 43 *Circular dichroism spectroscopy* 44

45
46 CD spectra were recorded at Jasco J-815 spectropolarimeter and the temperature was
47
48 controlled with PTC-423S temperature controller. A quartz cell with 1 cm optical path was
49
50 used. The spectra range was 190-260 nm with a resolution of 0.1 nm and a bandwidth of 1
51
52 nm. A scan speed of 20 nm/min with 1 s response time was employed. Baseline spectra were
53
54 subtracted from each spectrum and data were smoothed with the Savitzky-Golay method.
55
56 Data were processed using Origin 7.0 spread sheet/graph package. The direct CD
57
58
59
60

1
2
3 measurements (θ , in millidegrees) were converted to mean residue molar ellipticity, using the
4 relationship mean residue $\Delta\epsilon = \theta / (33000 \times c \times l \times \text{number of residue})$. 10 μM solution of *apo* and
5 metal (Ag (I) and Hg (II)) bound Bri2-23 either in phosphate buffer (50 mM) and at acidic pH
6 (~3.0) were analyzed.
7
8
9
10

11 *Potentiometry*

12
13
14
15 Stability constants for protons and Hg(II) complexes of cysteine and BRI2-23 were calculated
16 from titration curves carried out at 298K using a total volume of 1.5 cm^3 . The metal ion
17 concentration was $5 \times 10^{-4} \text{ mol} \times \text{dm}^{-3}$ and the metal to ligand ratio was 1:2. Competition
18 experiments were carried out with $5 \times 10^{-4} \text{ mol} \times \text{dm}^{-3}$ BRI2-23 peptide in the presence of 1
19 equivalent of cysteine and 1 equivalent of Hg(II) after 1 hour of equilibration time was
20 allowed before the titration started. NaOH was added from a 0.500 cm^3 micrometer syringe
21 which was calibrated by both weight titration and the titration of standard materials. The pH-
22 metric titrations were performed at 298K in 0.1 mol dm^{-3} NaCl on a MOLSPIN pH-meter
23 system using a Mettler Toledo InLab semi micro combined electrode calibrated in hydrogen
24 concentrations using HCl.⁴³ The HYPERQUAD program was used for stability constant
25 calculations.⁴⁴ Standard deviations were computed by HYPERQUAD and refer to random
26 errors only. They are, however, a good indication of the importance of a particular species in
27 the equilibrium.
28
29
30
31
32
33
34
35
36
37
38
39
40
41
42
43
44

45 *Isothermal titration calorimetry*

46
47
48 Calorimetric titrations of the peptide with Hg(II) ions were performed by isothermal
49 titration microcalorimetry (ITC) using Nano-ITC Instrument (TA Instruments, USA).
50 Experiments were carried out at 298K in distilled water at pH 3.0. Peptide concentration was
51 0.5 mM (950 μL sample cell), while the metal ion concentration 5.0 mM (in the syringe). Both
52 solutions were degassed for at least 15 min. by using TA Instruments degassing station, and
53
54
55
56
57
58
59
60

1
2
3 then stored under nitrogen to minimize sample oxidation. Automated titrations were
4
5 performed until saturation, up to Hg(II)/peptide mole ratio of about 3. Experiment was
6
7 repeated three times. Heats of dilution and mixing for each experiment were measured by
8
9 titrating Hg(II) solution into distilled water at pH 3.5. The effective heat of each peptide metal
10
11 ion interaction was corrected for dilution and mixing effects. Heats of bimolecular
12
13 interactions were obtained by integrating the peaks of each injection. The data were analyzed
14
15 using the NanoAnalyze software v. 2.3.6, using “multiple sites” binding model. ΔH° and the
16
17 corresponding binding constant, K_a , molar free energy of binding, ΔG° , and the molar entropy
18
19 change, ΔS° , were attained from the fundamental equations of thermodynamics: $\Delta G^\circ = -RT$
20
21 $\ln K_a = \Delta H^\circ - T(\Delta S^\circ)$.

22 23 24 25 26 *Perturbed Angular Correlation Spectroscopy*

27
28
29 The following stock solutions were prepared and used for the PAC experiments:
30
31 BRI2-23 (2 mM, concentration determined by the Ellman’s test),⁴⁵ phosphate buffer of pH 3.0
32
33 and pH 7.5 (0.93M, and HgCl₂ (3.0 mM). The final samples contained 50 mM of the proper
34
35 buffer, 200 μ M or 100 μ M BRI2-23, 100 μ M of HgCl₂ in 55% sucrose. Water (150 mL)
36
37 treated so as to lower the concentration of metal ions was placed in a small teflon cup sitting
38
39 on a copper device, frozen in liquid nitrogen and mounted at the ISOLDE GLM beam line (at
40
41 CERN) in a vacuum chamber. Radioactive ^{199m}Hg was implanted in the ice typically for 1
42
43 hour. The radioactive ^{199m}Hg was produced by irradiating a liquid lead target with 1 GeV
44
45 protons and selected using an on line mass separator. Detailed information regarding sample
46
47 preparation and data collection followed the protocol described in Iranzo et al.⁴⁶

48
49
50 Fits were carried out with 300 points disregarding the first 10 points due to systematic errors
51
52 in these, 0.05038 ns/channel, 0.981 ns time resolution. The pH presented in the table is the pH
53
54 in the sample at 274 K.
55
56
57
58
59
60

NMR Spectroscopy

NMR experiments were carried out at 14.1 T at controlled temperature (± 0.1 K) on a Bruker Avance 600 MHz equipped with a Silicon Graphics workstation. Suppression of residual water signal was achieved by excitation sculpting, using a selective square pulse on water 2 ms long. Proton resonance assignment was obtained by TOCSY and NOESY experiments. HSQC experiments were carried out with standard pulse sequences. Spectral processing was performed on a Silicon Graphics O2 workstation using the XWINNMR 3.6 or TOPSPIN 3.1 software. Solutions of *apo* and metal (Ag(I) and Hg(II)) bound Bri2-23 0.3mM either at acidic (~ 3.0) and physiological pH were analyzed. The intensities of NOESY cross-peaks, referenced to cross-peaks related to proton pairs at fixed distances were converted into proton-proton distance constraints; the constraints were used to build a pseudopotential energy for a restrained simulated annealing (SA) calculation in torsional angle space. In particular, we performed the calculation with the program DYANA,⁴⁷ with 300 random starting structures of the peptide and 10000 steps of SA.

Molecular Dynamics Simulations

The MD simulations were performed with the GROMACS 3.3.0 software package⁴⁸ using the GROMOS 96 force field⁴⁹ and the flexible SPC water model. The initial structure was immersed in a periodic water box of triclinic shape (1.50 nm thickness) and neutralized with 1 CL⁻ counterion. Electrostatic energy was calculated using the particle mesh Ewald method.⁵⁰ Cutoff distances for the calculation of the Coulomb and Van der Waals interaction were 0.9 and 1.0 nm, respectively. After energy minimization using a steepest decent method, the system was subject to equilibration from 0 to 298 K and normal pressure for 30 ps. The system was coupled to the external bath by the Berendsen pressure and temperature coupling.⁵¹ No positional restraint was given, only two distance restrain for the Cys5-Cu(I) and

1
2
3 Cys 22-Cu(I) binding (low = 1.8, up1= 2.3, up2 = 2.5). An average structure was refined
4 further using a steepest decent energy minimization. For simulating the Cysteine-copper(I)
5 bond, CYS2 residue were selected instead of CYS residue in Gromos 43a2 force field to
6
7 mimic the oxidized form, ready for metal ion binding. Moreover Arginine (+), Histidine (+)
8 and Lysine (+) were considered in the protonated form like in acidic pH, the total charge of
9 the peptide with Cu(I) ion was of 1+.

10
11
12
13
14
15
16 The starting point of the MD simulation analysis were the NMR output structures obtained
17 through the program DYANA after integrating the NMR 2D NOESY spectra to obtain
18 structural constrains. Seven of the best 30 DYANA structures were randomly selected as the
19 starting points for MD simulation. The Cys-Me binding site was firstly minimized with the
20 steepest descend method to obtain the estimated distance between copper and the cystein
21 sulfur. The distance restrains were then applied as constrains for MD simulation analysis
22 using the correct Force Field for this type of Me-bounded cysteines (CYS2 for gromos43a1).

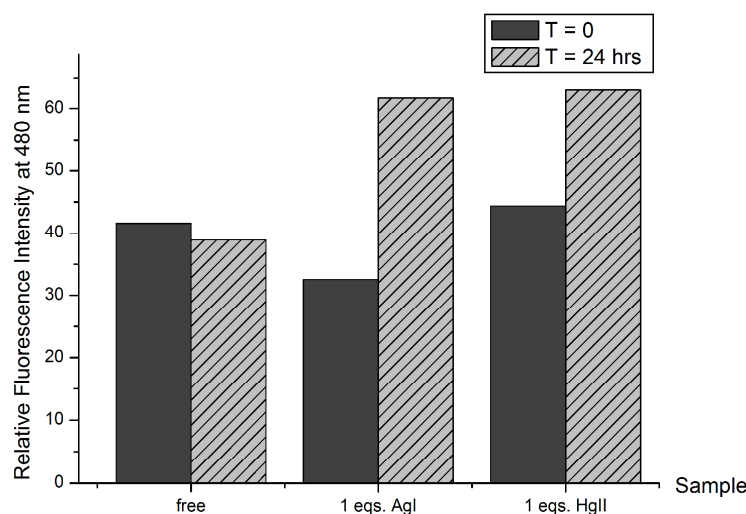
23
24
25
26
27
28
29
30
31
32
33
34
35
36
37
38
39
40
41
42
43
44
45
46
47
48
49
50
51
52
53
54
55
56
57
58
59
60
100ns of simulation was performed for each structure to reach the RMSD convergence and
maintain it for at least 20ns. The seven analyzed structures do not quickly reach the RMSD
stabilization, so during the 50ns of simulation a steepest descend energy minimization was
done every 5ns, also because of the undefined positional restrain given to the system and
because of the intrinsic unstructured part of the peptide.

Results

ThT fluorescence spectroscopy assay

The thioflavin-T (ThT) fluorimetric assay is widely used to underline the presence of
stable β sheet secondary structure for peptides or proteins.^{52,53} It is also known, especially for
amyloidogenic peptides, that a steady increase over time of the ThT fluorescent signal can be

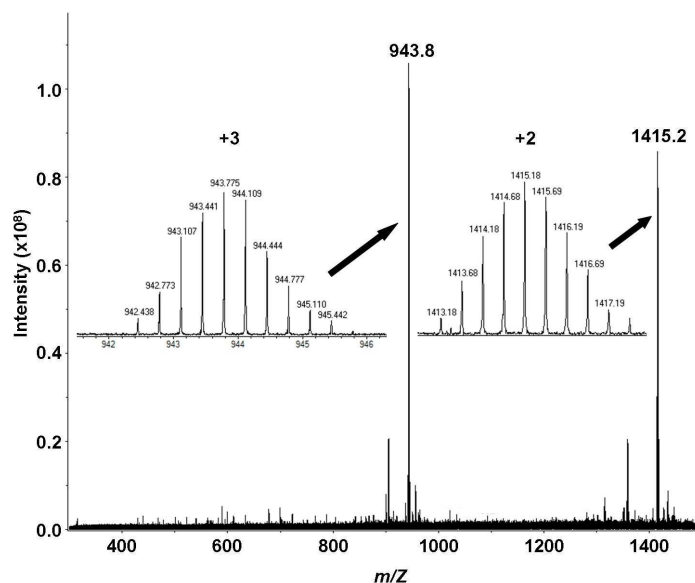
1
2
3 correlated to formation of precipitating complexes. In order to compare the β sheet structural
4 propensity of the peptide Bri2-23, the variation of ThT fluorescence of Bri2-23 peptide in
5 presence and in absence of Ag(I) and Hg(II) metal ions was analyzed. Immediately after the
6 metal additions, similar values of ThT fluorescence were measured (Figure 2). On the
7 contrary the same experiments repeated after 24 hours showed an increase of ThT
8 fluorescence of Bri2-23 solutions containing metal ions only. In particular, at $t=24$ hours, the
9 *apo* peptide gave almost the same ThT fluorescence as measured at $t=0$, while the binding to
10 Ag(I) or Hg(II) ions resulted in 30-50% of fluorescence enhancements. This behavior
11 supports the propensity of the metal bound Bri2-23 peptide to form β sheet structure in
12 solution, and confirms that a similar structural reorganization of the peptide is induced by
13 Ag(I) and Hg(II).
14
15
16
17
18
19
20
21
22
23
24
25
26
27
28
29
30
31
32
33
34
35
36
37
38
39
40
41
42
43
44
45



46 Figure 2. Relative fluorescence ThT intensity at 480 nm measured at $t=0$ and $t=24$ hrs in
47 50mM phosphate buffer for free Bri2-23 10 μ M and in presence of 0.7 equivalents of Ag(I)
48 and Hg(II), respectively; $c_{\text{ThT}} = 10 \mu\text{M}$.
49
50
51
52
53
54
55
56
57
58
59
60

Mass spectrometry

1
2
3 The results of mass spectrometric analyses indicate that at slightly acidic pH
4 conditions *apo* BRI2-23 (data not shown) and its mercurated complex ($m/Z = 943.8$ and
5 1415.2) exist as monomers (Figure 3). No species of higher ligand content with respect to
6 metal have been detected, but this may be because it is difficult to detect polymeric forms of
7 ligand or its complexes. To reduce the system's aggregation susceptibility in the presence of
8 metal, the mixture used in experiments contained 10% of DMSO. Interestingly, in absence of
9 DMSO (data not shown) no spectra was obtainable for the peptide in the presence of Hg(II),
10 possibly indicating aggregation. The MS data can be modeled with doubly deprotonated
11 BRI2-23 and one Hg(II) ion bound, presumably reflecting coordination by the two thiolates.
12
13
14
15
16
17
18
19
20
21
22
23
24
25
26
27
28
29
30
31
32
33
34
35
36
37
38
39
40
41
42



43
44 Figure 3. ESI-MS spectra of Hg(II) complex of BRI2-23 peptide at pH 6.5 in carbonate buffer
45 (1mM). $C_{\text{BRI2-23}} = 1 \times 10^{-4} \text{M}$; Hg(II)/BRI2-23 ratio 1:1; MeOH/H₂O/DMSO = 9:9:2.
46
47

48 49 *Circular dichroism spectroscopy*

50
51 At both physiological and acidic pH *apo* Bri2-23 displays typical random coil CD
52 spectra (Figure 4A), with the main absorption at 198 nm characteristic of flexible and
53 disordered protein.⁵⁴ Upon Hg(II) and Ag(I) addition the CD spectra undergo changes in both
54
55
56
57
58
59
60

the shape and in the wavelength of the main adsorption bands (Figures 4B and 4C). The two metals gave very similar changes, showing a negative absorption at 208-210nm. The difference spectra (Figure 4D) obtained by subtracting the CD spectra of the *apo* peptide from the metal complexes have the typical shape of those of β sheet proteins, thus supporting the ThT results indicating that Bri2-23 forms β sheet structure in presence of both Hg(II) and Ag(I) ions. It cannot be excluded that the CD spectroscopic changes originate from LMCT bands appearing upon the binding of the metal ions to BRI2-23. However, the change towards a β sheet like spectrum upon metal ion binding is remarkable, and appears qualitatively similar for both metal ions.

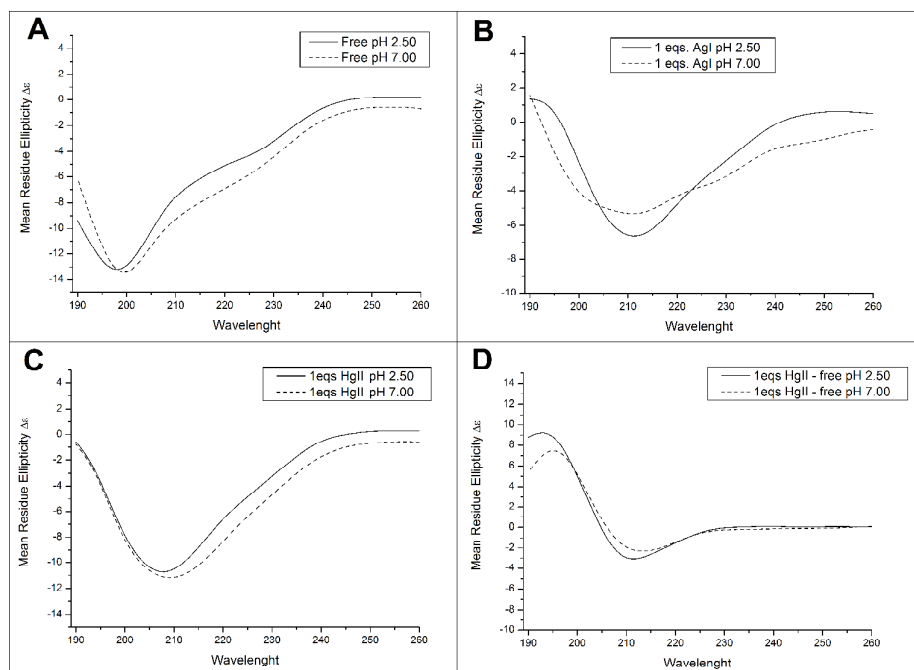


Figure 4. CD spectra recorded at pH 2.5 (3mM HCl) and 7.0 (50mM phosphate buffer) for 10 μ M *apo* Bri2-23 (A), 10 μ M Bri2-23 in presence of 1.0 equivalents Ag(I) (B); 10 μ M Bri2-23 in presence of 1.0 equivalents Hg(II) (C) and difference CD spectra for mercurated peptide and its *apo* form (D).

Potentiometric studies

Potentiometric titration reflects that in the measured pH range unprotected EASNCFAIRHFENKFAVETLICS peptide (BRI2-23) behaves like H₉L acid (Table1). The nine protonation constants correspond to consecutive proton binding to ε-amino group of Lys, thiolate groups of two Cys, terminal α-amino group, imidazole nitrogen of His, γ-carboxylate of three glutamate residues and terminal α-carboxylate group. The protonation of guanidinyll function of Arg residue cannot be followed.

Table 1. Protonation constants for 1mM BRI2-23 peptide and cysteine at T = 298.2 K and I = 0.1 M in NaCl; $c_{\text{BRI2-23}} = 1 \times 10^{-3}$, $c_{\text{Cys}} = 1 \times 10^{-3}$.

Species	logβ	log K	Residue
<i>BRI2-23</i>			
HL	10.05(2)	10.05	Lys
H ₂ L	19.48(2)	9.43	Cys
H ₃ L	28.04(3)	8.57	Cys
H ₄ L	35.62(1)	7.58	αNH ₂
H ₅ L	41.98(5)	6.36	His
H ₆ L	46.74(6)	4.76	Glu
H ₇ L	50.87(7)	4.13	Glu
H ₈ L	54.37(7)	3.50	Glu
H ₉ L	57.38(9)	3.01	αCOO-
<i>cysteine</i>			
HL	10.21(1)	10.21	αNH ₂
H ₂ L	18.45(1)	8.24	SH
H ₃ L	20.57(1)	2.12	αCOO-

Table 2. Stability constants for the Hg(II) complexes of cysteine, BRI2-23 and their ternary complexes at Hg(II)/BRI2-23/cysteine ratio 1:1:1; T = 298.2 K and I = 0.1 M in NaCl; $c_{\text{BRI2-23}} = 5 \times 10^{-4}$, $c_{\text{Cys}} = 5 \times 10^{-4}$, $c_{\text{Hg(II)}} = 5 \times 10^{-4}$.

Species ^a	logβ	log K	log K ^{*b}
HgH ₃ Cys ₂	62.51(1)		
HgH ₂ Cys ₂	60.04(1)	2.47	
HgH ₁ Cys ₂	52.44(1)	7.60	
HgH ₀ Cys ₂	43.57 [#]	8.87	
HgH ₋₁ Cys ₂	33.51(1)	10.06	

HgH ₆ L	54.86(12)		0.49
HgH ₅ L	51.97(11)	2.89	1.10
HgH ₄ L	48.55(12)	3.42	1.81
HgH ₃ L	43.91(11)	4.64	1.94
HgH ₂ L	37.72(12)	6.19	2.10
HgH ₂ CysL	52.85(6)		
HgHCysL	43.92(6)	8.93	
HgCysL	34.10(6)	9.82	

^a L indicates BRI2-23 peptide as a ligand; ^b $\log K^* = \log \beta(\text{CuH}_j\text{L}) - \log \beta(\text{H}_n\text{L})$ (where the index j corresponds to the number of the protons in the coordinated ligand to metal ion and n corresponds to the number of protons coordinated to ligand).

[#] Data adapted from Stricks and Kolthoff⁵⁵

Since mercury(II) is known of its extreme high affinity to sulfhydryl-containing ligands,^{55,56} the reasonable explanation of the interactions between the BRI2-23 ligand and Hg(II) obligate us to emphasize that the total complexation of the metal ion with this ligand is essentially complete below pH 2. Therefore, complex formation constants could not be determined directly from potentiometric titration and a competitive potentiometric experiments were carried out with cysteine as competitor ligand under our experimental conditions.⁵⁷ First, the protonation constants for cysteine were determined from potentiometric titrations followed by determination of stability constants for its mercuric complexes where the formation constant reported by Stricks and Kolthoff for Hg(Cys)₂ species was used as the fixed value.⁵⁵ Constants determined for cysteine can be assigned to amine (10.21), thiolate (8.24) and carboxylate (2.12) protonations (Table 1). As in previous studies⁵⁷ five complex species have been found within measured pH range all engaging two ligands in Hg(II) sequestration (Table 2). Subsequently, potentiometric titration at a 1:1:1 Hg(II)/Cys/BRI2-23 ratio were carried out. Slow stabilization in the competition region resulted in relatively high standard deviations reported for the calculated complex species. The best fit results are presented in Table 2. Comprehensive analysis of potentiometric data reveals the presence of 13 complex species, five (HgH₃Cys₂, HgH₂Cys₂, HgHCys₂, HgCys₂, HgH₋₁Cys₂) representing binary Hg(II)

species of cysteine, five binary complexes of mercury(II) bound BRI2-23 (HgH_6L , HgH_5Bri , HgH_4Bri , HgH_3Bri , HgH_2Bri) and three ternary complex species (HgH_2CysL , HgHCysL , HgCysL) that coexist in alkaline pH range (Figure 5).

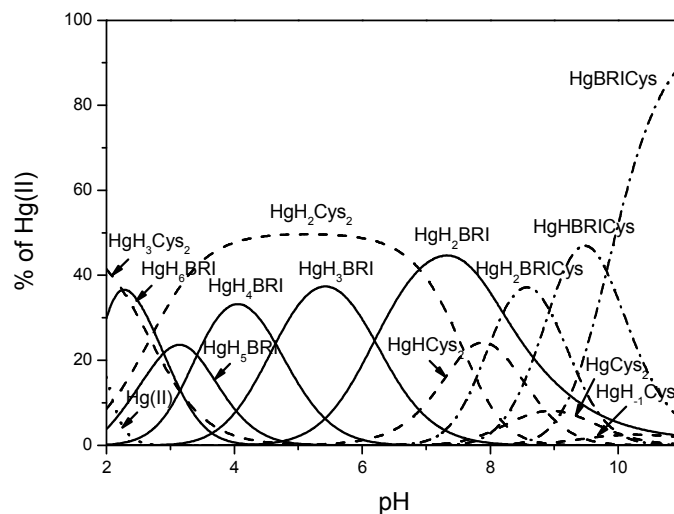


Figure 5. Species distribution diagram for Hg(II) complexes of BRI2-23 peptide in the presence of Cys at a 1:1:1 Hg/BRI2-23/Cys ratio; $T = 298.2 \text{ K}$ and $I = 0.1 \text{ M}$ in NaCl ; $c_{\text{BRI2-23}} = 5 \times 10^{-4}$, $c_{\text{Cys}} = 5 \times 10^{-4}$, $c_{\text{Hg(II)}} = 5 \times 10^{-4}$.

Although BRI2-23 is a moderately weak competitor of cysteine, we are able to determine stability of its mercuric complexes in ternary system. Usually, the most reliable measure that allows for direct assessment of affinity of various ligands toward metal ion is $\log K^*$, protonation corrected stability constant.⁵⁸ Taking into account the relatively high standard deviation we are able to quantify the $\log K^*$ for BRI2-23 Hg(II) complexes to vary between 0.5 and 2. This discrepancy is the consequence of structural rearrangements of peptide chain that mutually result from metal binding and changes in proton concentration. Extensions of peptide sequence with structure-rearranging domain usually increase the stability of its metal complexes.^{59,60} Analogous estimate of $\log K^*$ for cysteine complexes of general formula HgH_xCys_2 gives value exceeding 23. In consequence BRI2-23 could hardly compete with cysteine for Hg(II) binding. Furthermore, if this measure is critical factor, such a high

1
2
3 difference in stability would abolish formation of ternary complexes that have been
4
5 determined by potentiometric titrations. Against all odds, mass spectrometric analysis
6
7 confirms the occurrence of ternary complexes in alkaline pH range (see figures 1S and 2S for
8
9 details).

10
11
12 The experiments performed in ternary system has been followed by corresponding
13
14 titrations carried out for binary system with the aim of testing the system's behavior in
15
16 absence of any competing ligand. As we know from competition experiments, BRI2-23 is
17
18 hardly able to compete with cysteine for metal binding in wide pH range. To reproduce the
19
20 constraints of ternary system and to keep the homogeneity of the complex species formed in
21
22 solution (*vide supra*) metal pool accessible for BRI2-23 sequestration was kept at a half of the
23
24 concentration of ligand. Moreover, formation constant calculated for HgH₂BRI complex was
25
26 used as the predetermined value. The best fit results are shown in Table 3. Analysis of
27
28 potentiometric data reveal the formation of seven complex species HgH₆L, HgH₅L, HgH₄L,
29
30 HgH₃L, HgH₂L, HgHL and HgL (Figure 6). Stability constants for corresponding complex
31
32 species formed in acidic and neutral pH range correlate well with values calculated for ternary
33
34 system (Table 2), while formation constants for species HgHL and HgL, present in alkaline
35
36 pH range give reasonable log K* values. In addition, available potentiometric, mass
37
38 spectrometric and NMR data do not indicate formation of complex species with two ligand
39
40 molecules binding Hg(II) (Figure 6).
41
42
43
44
45

46
47 Table 3. Stability constants for the Hg(II) complexes of BRI2-23 at Hg(II)/BRI2-23 ratio 1:2;
48
49 T = 298.2 K and I = 0.1 M in NaCl; c_{BRI2-23} = 1x10⁻³, c_{Hg(II)} = 5x10⁻⁴.

Species ^a	logβ	log K	log K* ^b
HgH ₆ L	55.10(2)		0.73
HgH ₅ L	52.09(1)	3.01	1.22
HgH ₄ L	48.65(1)	3.44	1.91
HgH ₃ L	44.01(1)	4.64	2.03
HgH ₂ L	37.72 [#]	6.29	2.10

HgHL	29.54(1)	8.18	1.49
HgL	18.59(2)	10.95	0.59

^a L indicates BRI2-23 peptide as a ligand

^b $\log K^* = \log \beta(\text{CuH}_j\text{L}) - \log \beta(\text{H}_n\text{L})$ (where the index j corresponds to the number of the protons in the coordinated ligand to metal ion and n corresponds to the number of protons coordinated to ligand).

[#] Calculated in ternary system.

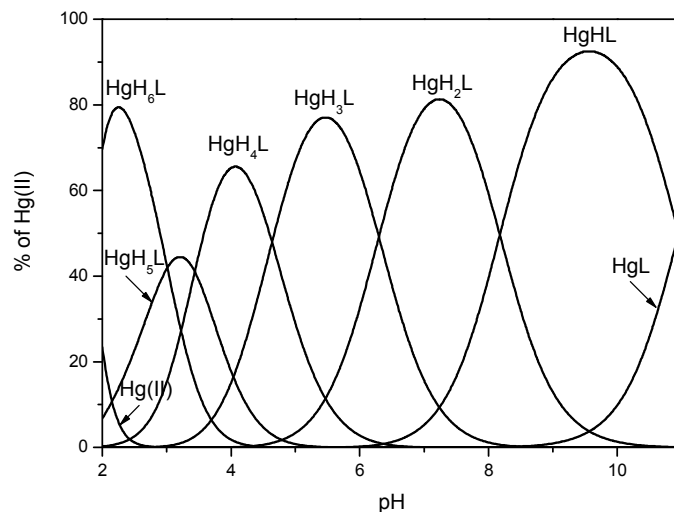


Figure 6. Species distribution diagram for Hg(II) complexes of BRI2-23 peptide in the at a 1:2 Hg/BRI2-23 ratio; $T = 298.2 \text{ K}$ and $I = 0.1 \text{ M}$ in NaCl; $c_{\text{BRI2-23}} = 1 \times 10^{-3}$, $c_{\text{Hg(II)}} = 5 \times 10^{-4}$.

Isothermal titration calorimetry

As we know from potentiometric experiments the total complexation of the metal ion with BRI2-23 is essentially complete below pH 2 and subsequent complex species differ only in the protonation state of groups not involved in Hg(II) binding. Therefore, comprehensive thermodynamic analysis of the interaction of BRI2-23 with Hg(II) by the isothermal titration calorimetry experiments have been performed in acidic pH range (see supplementary information for details).

Perturbed angular correlation spectroscopy (PAC)

$^{199\text{m}}\text{Hg}$ PAC spectroscopy was conducted in order to elucidate the metal site coordination geometry. The PAC parameters derived from analysis of the experimental data, Figure 4S and 7, are summarized in Table 1S. With a peptide:Hg(II) stoichiometry of 2:1 at pH 3.0 one nuclear quadrupole interaction (NQI) dominates the spectra. This NQI compares well with previous observations of HgS_2 coordination geometries.⁴⁶ The same NQI is dominating at peptide:Hg(II) stoichiometry of 1:1 at pH 3.0. At pH 7.4 the signal is still dominated by that of the HgS_2 coordination geometry, but it changes slightly, with line broadening especially of the second peak at ~ 2.7 rad/ns, and a minor decrease in frequency. The line broadening implies either internal dynamics at the metal site or that more than one NQI, and thus more than one coordination geometry, is present. Thus, a second NQI was introduced in the data analysis, see Table 1S, and the fitted parameters fall in-between reference data for HgS_2 and HgS_3 model systems, and might indicate that a fraction of the Hg(II) ions are in coordination geometries with coordination number higher than 2.⁴⁶ The analysis is difficult, and other fits of equal quality may exist.

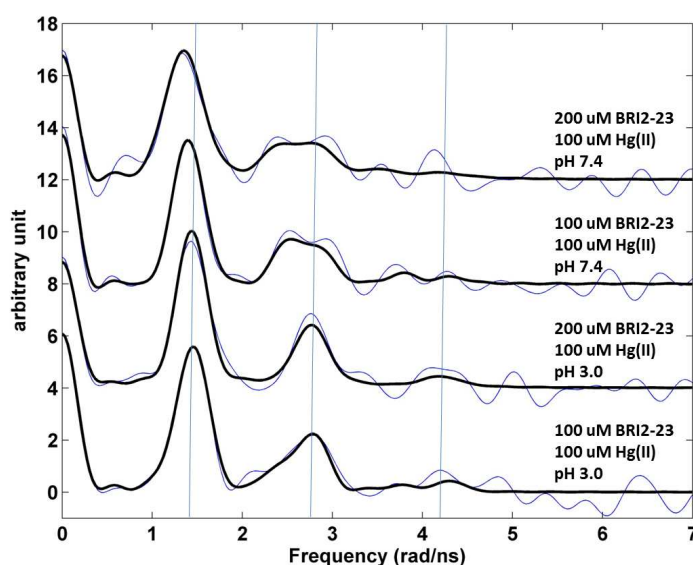


Figure 7: Fourier transformed $^{199\text{m}}\text{Hg}$ PAC data for BRI2-23 in 50mM phosphate buffer, pH 3.0 or 7.4 with addition of sucrose (55%); $c_{\text{Hg(II)}} = 1 \times 10^{-4}$ M, Hg(II)/BRI2-23 ratio 1:1 or 1:2. Blue: Fourier transformed experimental data; Black: Fit with the parameters presented in

1
2
3 Table 1S. Vertical blue lines are added to aid the eye, at the frequencies recorded at pH 3.0
4 with 2:1 BRI2-23 to Hg(II) stoichiometry, reflecting a typical HgS₂ coordination geometry.
5
6

7
8 *Nuclear Magnetic Resonance spectroscopy*
9

10
11 In order to characterize the metal coordination sphere of Bri2-23 and to better
12 understand the conformational rearrangements of the peptide, the NMR behavior of both *apo*
13 and metal bound forms was analyzed. Addition of Ag(I) or Hg(II) ions yielded very similar
14 NMR spectra (Figure 5S), suggesting similar coordination features for both metals. However,
15 the spectra of the silver complex were broader than the mercury ones, such that successive
16 analyses were carried out on of Hg(II) systems only.
17
18
19
20
21
22
23
24

25 Hg(II) titration experiments were performed to determine the metal binding
26 stoichiometry, up to 1.8. Hg(II) equivalents were added to Bri2-23 solutions. Hg(II) additions
27 up to 0.9 equivalents resulted in change of NMR parameters of selected proton and carbon
28 NMR resonances, on the contrary higher metal concentrations did not significantly further
29 affect the spectra, except for increased line broadening of NMR signals, probably due to the
30 presence of intermolecular species or soluble aggregates. The addition of 0.5 Hg(II)
31 equivalents causes the reduction of NMR resonances belonging to the *apo* form with the
32 simultaneous appearance of new peaks corresponding to the metal-bound form (Figure 8A),
33 indicating the occurrence of a slow exchange regime (respect to the NMR time scale) between
34 the free and bound states. The presence of both *apo* and metal bound signals observed at that
35 condition strongly indicate that 1:1 complexes, rather than bis-complexes, are formed. Further
36 addition of Hg(II) results in (i) the complete disappearance of the NMR resonances of the *apo*
37 Bri2-23 and (ii) an increase of the intensity of the peaks corresponding to the metal complex
38 (Figure 8B). Furthermore, the correlations observed upon the addition of 0.5 metal
39 equivalents are well superimposed to those corresponding to either the free or metal bound
40
41
42
43
44
45
46
47
48
49
50
51
52
53
54
55
56
57
58
59
60

Bri2-23 (Figure 6S). In addition, the NMR spectra revealed the occurrence of two Hg(II) bound forms in slow exchange respect to the NMR time scale. The two forms (hereafter called form X and Y) exhibited clear and diverse NMR signals for residues 9-21, while showed similar chemical shift for the first 8 residues. From the evaluation of the relative intensities of the NMR signals belonging to the two bound forms, the form X was found to be more abundant than the other. The full ^1H assignments of Bri2-23 and the two Hg(II) bound forms (X and Y) are reported in Tables 2S, 3S and 4S).

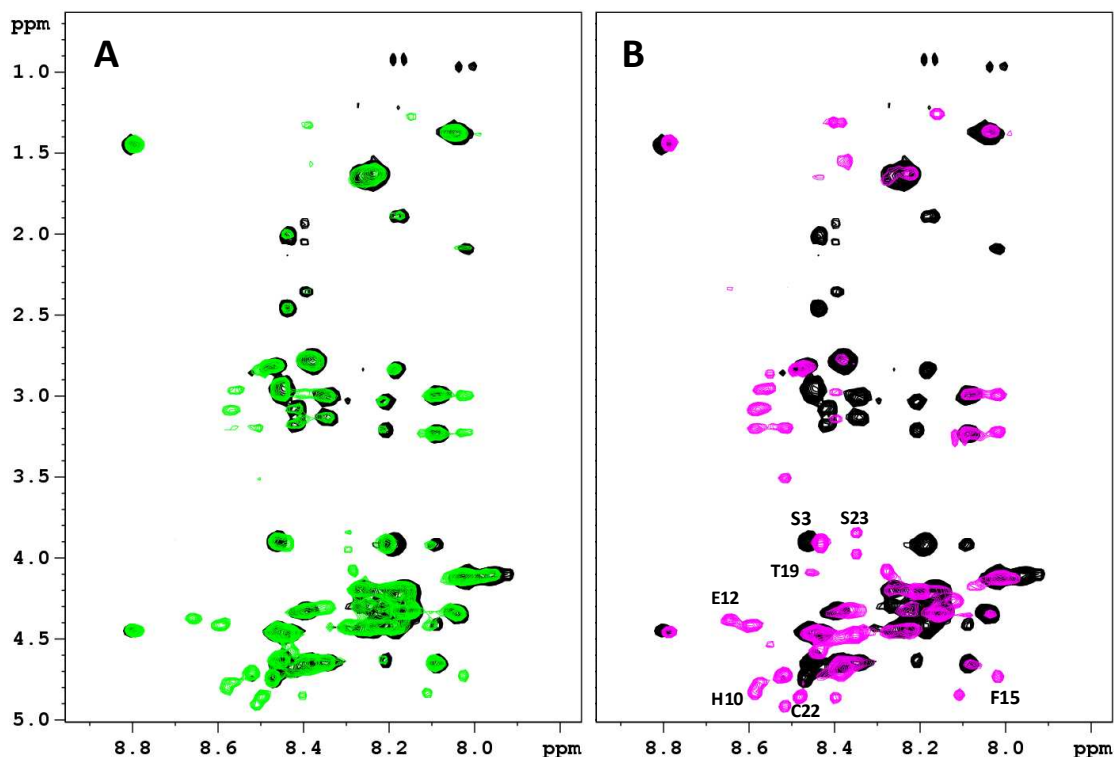


Figure 8. 2D ^1H - ^1H TOCSY spectra (NH-H α region) of Bri2-23 0.5mM in H $_2$ O:D $_2$ O 90:10 at 298K and pH 3.0 in presence of A) 0.5 equivalents of Hg(II) ions; B) 0.7 equivalents of Hg(II) ions.

After the complete assignment of the NMR spectra of the *apo* and Hg(II) bound Bri2-23 forms, the Chemical Shift Index (CSI) and the Chemical Shift Variation induced by the metal

ion for the most abundant species (form X) was calculated. The CSI, calculated on the chemical shift of the H α protons, is reported in Figure 9. The results obtained for the *apo* peptide confirm the random coil nature of Bri2-23, as previously detected from CD analysis. On the other hand the CSI obtained for the metal bound form demonstrates a behavior typical of a β strand structured peptide, especially for the regions from Asn-4 to Arg-9 and from Val-17 to Cys-22. Similar results were obtained by the analysis of the chemical shift variation induced by Hg(II) on NH and H α protons (Figure 10). Both metal bound forms show large chemical shift variations, especially in the regions from 4 to 8 and from 16 to 22. In order to better determine the metal binding donor atoms, the Hg(II) induced chemical shift variations on all of side-chain protons were calculated as well (Figure 10). The protons exhibiting the largest changes belong to H β of both Cys-5 and Cys-22, strongly supporting the metal coordination to thiolate groups.

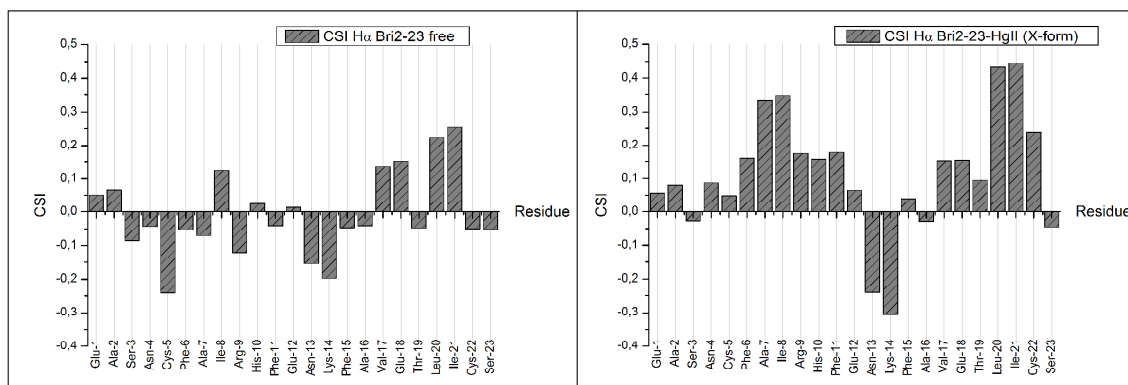


Figure 9. Chemical Shift Index of Bri2-23 *apo* form (A) and of the most abundant Hg(II)/Bri2-23 complex X (B).

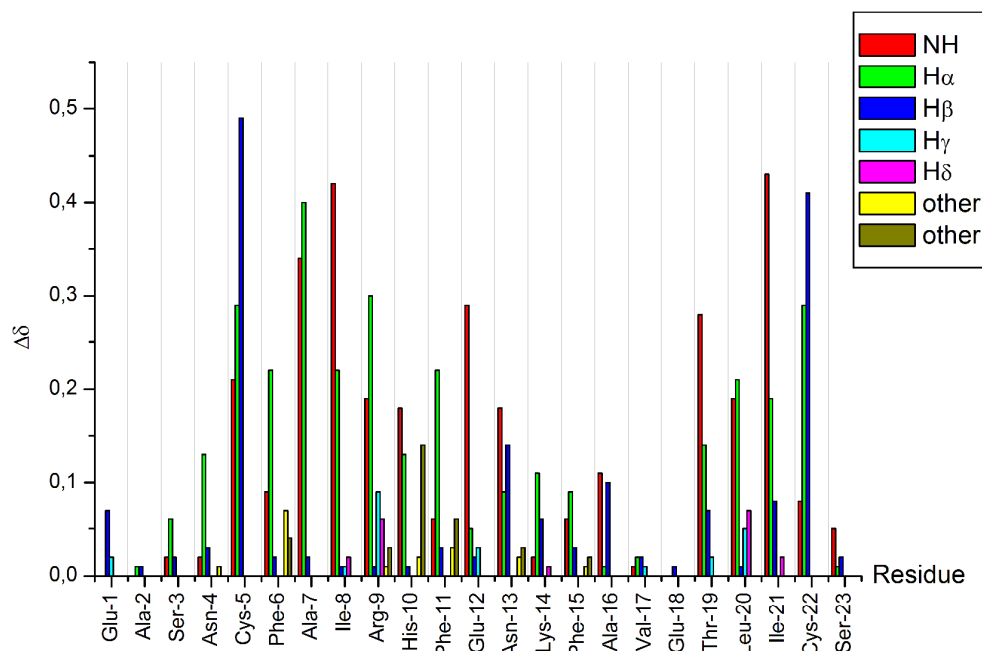


Figure 10. Chemical Shift Variation induced by Hg(II) on Bri2-23 protons.

The analysis of 2D ^1H - ^1H NOESY spectra was also performed in order to determine the three dimensional structure the Bri2-23-Hg(II) complex. 70 NOEs were thus converted in proton-proton distance constraints to be used for structure calculation by using the DYANA program. However no a clear cut arrangement of the peptide was obtained from those calculations (bb-RMSD: 4.38 +/- 0.94 Å, and an average target function of 1.08 +/- 0.023).

Molecular Dynamics Simulations

The structural propensity of the Bri2-23-Hg(II) complex was investigated by Molecular Dynamics Simulations (MD) performed on seven random structures selected from the thirty ones generated from DYANA calculation (Figure 7S). Combination of experimental and theoretical techniques has been previously applied to investigate metal binding to amyloidogenic model peptides.⁶¹⁻⁶⁴ For each of the seven structures shown, a 100ns of MD

1
2
3 simulation was performed using the simulation program GROMACS³¹. Contrary to the NMR
4
5 analysis, we decided to run MD by considering Cu(I) instead of Hg(II) or Ag(I) as the metal
6
7 bound ion. This choice was mainly due to the fact that Cu(I) is the real metal of interest and
8
9 that Hg(II) and Ag(I) were just used as probes for Cu(I) in the spectroscopic analysis. Among
10
11 the seven analyzed structures only five easily reached bb-RMSD convergence after 100 ns
12
13 (Figure 11, structures A, B, C, D and G). The stability of each simulated systems was
14
15 controlled also through the output pdb files, where backbone overlap occurred in the last 20
16
17 ns confirming the secondary structure stability (Figure 11). For structures E and F, after 100
18
19 ns of simulation, bb-RMSD did not converge. This can happen when i) the system attains a
20
21 random coil secondary structure, so the bb will not be stable at all, or ii) the major part of the
22
23 bb remain stable over time while the C-and N-terminus (which could be the random part of
24
25 the sequence) have a high mobility. To monitor this behavior the fluctuation of single residues
26
27 over time was calculated for structures E and F. As shown in Figure 8S, we found that the N-
28
29 and C-termini are much more unstable than the central part of the sequence (especially for
30
31 structure F). For these reasons we decided to include in our analysis also the results obtained
32
33 from structures F and E.

34
35
36
37
38 Ribbon representations are shown in Figure 11. Structures A, B, C, E and G present a well
39
40 defined conformation, composed by a short N- and C-termini random part, followed by a
41
42 short β -sheet (parallel or anti-parallel) and a central domain constituted by turn and bend
43
44 elements. In contrast, structures D and F do not possess an intrinsic β -sheet frame, and they
45
46 just show the features of a simple but well organized conformation characterized by bend,
47
48 turn and β -bridge secondary structure.
49
50
51
52
53
54
55
56
57
58
59
60

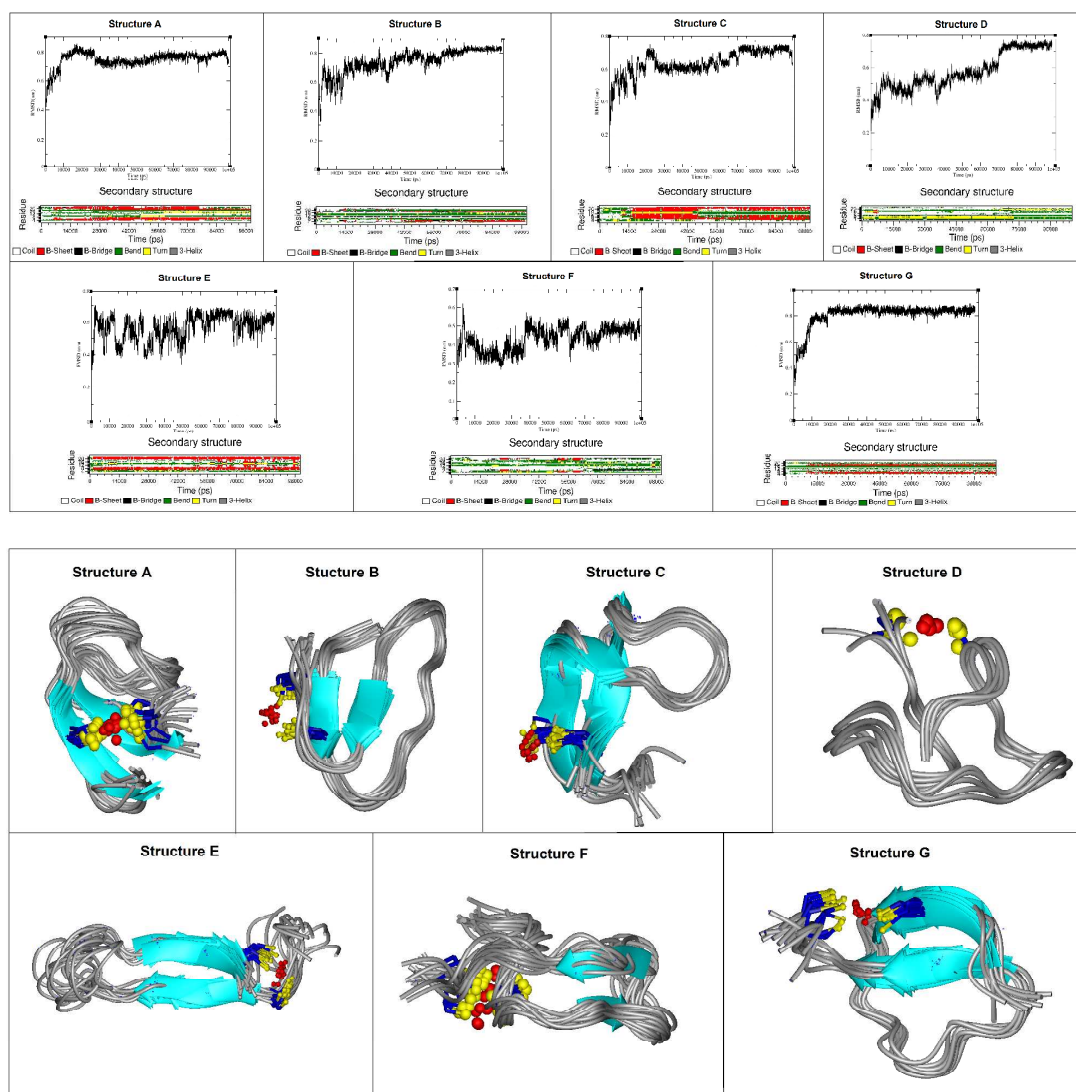


Figure 11. Backbone RMSD, secondary structure evolutions as function of time. (upper panel) and the snapshots from the last part of the MD trajectories of Hg(II)-BRI2-23 molecules (lower panel).

From a statistical point of view, 5 of the 7 analyzed structures show a well defined β sheet arrangement, demonstrating the high propensity of Cu(I) bound peptide to adopt a partial β sheet secondary structure, confirming the analysis of the CD, ThT and NMR experimental data (section 1, 2 and 3). The obtained data support the existence of a β sheet region located at the proximity of the metal binding site (Cys-5 and Cys-22). The amino acids involved in the β sheet formation are not unequivocally determined (see Table 5) suggesting the dynamic

nature of the system. Interestingly, the distance between the two sheets is constant, despite the structured part starts at Ser-3 or at Phe-6.

Table 5. Schematic representation of amino acid residues involved in β sheet formation.

Structure	Amino acid residues involved in 1 st strand	Amino acid residues involved in 2 nd strand
A	5 6	18 19
B	4 5	17 18
C	4 5 6 7 8 9 10	18 19 20 21 22
D		
E	6 7 8 9	19 20 21 22
F		
G	3 4 5 6	16 17 18

Discussion

Knowledge of metal binding properties of BRI2 and the products of its proteolytic cleavage is limited to one report related to metallochemistry of ABri, the amyloidogenic product of furin cleaved homologue of BRI2.²⁰ There are no similar studies for the wild type peptide (BRI2-23) that, contrary to its pathogenic homologue, does not aggregate and even effectively inhibits A β aggregation.

Our major interest was to examine the interaction of BRI2-23 with soft metal ions, by using Hg(II) and Ag(I) as Cu(I) probes, to assess the impact of metal sequestration on peptide structure and metal binding affinity at conditions where aggregation is disfavored. Hg(II) is known for very high affinity for thiolate containing ligands. Hg(II) binding to low molecular weight compound like cysteine, penicillamine, glutathione typically yields extremely stable

1
2
3 complex species. On the other hand, the selectivity of metal ion binding to peptides
4
5 containing two or more cysteinyl residues is strongly dependent on the distance between the
6
7 thiolates involved in metal ion sequestration,⁶⁵ over and above their conformational
8
9 orientation.^{57,66} Design of peptides that predispose binding thiolates into metal preferred
10
11 orientation yielded exceptionally stable complex species able to compete with low molecular
12
13 weight compounds in Hg(II) sequestration.⁵⁷
14
15

16
17 As demonstrated by the CD and NMR analyses *apo* BRI2 23 preferentially adopts random
18
19 conformation, which do not favors the intramolecular mercury(II) binding to Cys-5 and Cys-
20
21 22, separated by 16 amino acid residues. Nonetheless, BRI2-23 has the ability to form Hg(II)
22
23 mononuclear intramolecular species with a HgS₂ coordination geometry, as indicated by the
24
25 analysis of ESI MS data (Figure 3). The isotopic profile of the detectable species perfectly
26
27 matches the simulated mononuclear intramolecular HgBRI2-23 complex. Furthermore,
28
29 although PAC spectroscopy does not discriminate between the intra- or inter-molecular metal
30
31 site, it confirms the occurrence of HgS₂ coordination geometry in solution at low pH (Figure
32
33 7). Similarly, the large chemical shift changes observed for Cys-5, Cys-22 and residues
34
35 nearby, indicates that these residues are coordinated to Hg(II) in the predominant metal
36
37 complex (Figure 10). Interestingly, nearly exclusive intramolecular binding is observed at
38
39 metal ion concentrations not exceeding 0.5 molar equivalents with respect to the peptide, as
40
41 reflected by the NMR and potentiometric analysis (Figures 6 and 8). NMR analysis also
42
43 revealed the presence of two metal-bound species with form (X) still predominant in the
44
45 equilibrium. Relatively low concentration of minor species (Y) does not allow for its
46
47 comprehensive structural analysis.
48
49
50
51

52
53 As indicated by the large broadening of NMR signals and by the ITC experiments, further
54
55 increase of M:L ratios results in the evolution of metal-bridged oligomeric species (e.g.
56
57
58
59
60

1
2
3 Hg_m(BRI2 23)_n) that may coexist in solution with HgBRI2-23 macrochelates. This behavior
4
5 epitomizes previously detected pH dependent scrambling of ABri.⁶⁷
6
7

8 Our titration experiments indicate that Hg(II) interact with BRI2-23 in a concentration
9
10 dependent manner, yielding primarily a mixture of intramolecular macrochelate and
11
12 structurally undefined species that with metal concentration exceeding 0.7 Hg(II) equivalents
13
14 are converted into polymeric species of unknown structure and stoichiometry. Aggregates
15
16 giving response in ThT assays are formed, indicating that the presence of 0.7 Hg(II) or Ag(I)
17
18 equivalents does lead to aggregation (Figure 2).
19
20
21

22 The three dimensional structure of mononuclear BRI2-23 complex was
23
24 unapproachable directly from NMR data analysis. However, NMR provided reliable
25
26 constraints to molecular dynamics analysis. Nearly all MD trajectories present predominantly
27
28 β sheet arrangement of peptide structure upon metal binding in contrast to completely random
29
30 structure of free peptide (Figure 11). As indicated in Table 5, the residues involved in β -sheet
31
32 structure are not well defined. This behavior is consistent with a relative flexibility of the β -
33
34 sheet rearrangement and it is in agreement with the lack of precise NOEs constraints
35
36 unequivocally leading to the NMR structure of the metal complex. However, as supported by
37
38 the chemical shift analysis (Figure 9) and by the MD data (Figure 11), metal ion binding has
39
40 critical impact on molecular architecture of the peptide and enforces its refolding to yield
41
42 species of predominant β pleated sheet conformation, hence more prone to aggregation.
43
44 Although these species are not exactly the same in terms of proposed molecular architecture
45
46 of the peptide backbone, most of them resemble either parallel or antiparallel β -sheet rich
47
48 structures. The suggested conformational shift is additionally supported by changes of far-UV
49
50 profile of CD spectra demonstrating transition towards β -sheet arrangement of peptide
51
52 backbone (Figure 4).
53
54
55
56
57
58
59
60

1
2
3 Formation of oligomeric species observed at higher metal concentration may either
4 proceed through subsequent Hg(II) and peptide incorporation that yields expanded metal
5 bridged precipitate or alternatively represents the required core for BRI2-23 aggregation. The
6 time dependence and molecular mechanism of aggregation remains to be elucidated. In
7 consequence, metal ion sequestration may eradicate a key attribute of BRI2-23, its A β
8 aggregation inhibitory activity and/or even convert the peptide into an aggregation promoter.
9
10
11
12
13
14
15
16
17
18
19

20 Acknowledgements

21
22 We would like to thank National Science Center (NCN 2011/01/B/ST5/03936), PRIN
23 (Programmi di Ricerca di Rilevante Interesse Nazionale) (2010M2JARJ_004), CIRMMP
24 (Consorzio Interuniversitario Risonanze Magnetiche di Metalloproteine Paramagnetiche) and
25 CIRCMSB (Consorzio Interuniversitario di Ricerca in Chimica dei Metalli nei Sistemi
26 Biologici) for financial support. LH thanks ISOLDE/CERN for beam time grant IS488, and
27 for ENSAR support.
28
29
30
31
32
33
34
35
36
37
38
39

40 Electronic supplementary information (ESI) available:

41
42 Mass spectrometry analysis of ternary system; Fig. 1S, ESI-MS spectra of Hg(II)
43 complex of BRI2-23 peptide at pH 11 in ammonium hydroxide (0.4M). $c_{\text{BRI2-23}} = 1 \times 10^{-4}\text{M}$;
44 Hg(II)/BRI2-23/Cys ratio 1:1:1; MeOH/H₂O = 1:2. isothermal titration calorimetry studies;
45 Fig. 2S, Isotopic profile of ternary Hg(II) complex species of BRI2-23 and cysteine at pH 11
46 in ammonium hydroxide (0.4M). [BRI2-23] $1 \times 10^{-4}\text{M}$; Hg(II)/BRI2-23/Cys ratio 1:1:1;
47 MeOH/H₂O = 1:2; Isothermal titration calorimetry; Fig. 3S, Total measured heat associated
48 with titration of BRI peptide with Hg(II), and the binding isotherm derived from the enthalpy
49
50
51
52
53
54
55
56
57
58
59
60

1
2
3 of each injection in the function of molar equivalents of Hg(II); Fig. 4S, $^{199\text{m}}\text{Hg}$ PAC data for
4 BRI2-23 under the indicated experimental conditions; Fig. 5S. 2D ^1H - ^1H TOCSY spectra
5 (NH-H α region) of Bri2-23 0.5mM in H $_2\text{O}$:D $_2\text{O}$ 90:10 at 298K and pH 3.0 in presence of A)
6 0.9 equivalents of Ag(I) ions; B) 0.9 equivalents of Hg(II) ions; Fig. 6S, 2D ^1H - ^1H TOCSY
7 spectra of Bri2-23 0.5mM in H $_2\text{O}$:D $_2\text{O}$ 90:10 at 298K and pH 3.0, in presence of 0.5
8 equivalents of Hg(II) ions, in presence of 0.9 equivalents of Hg(II) ions; Fig. 7S,
9 Superimposed selected structures obtained by NMR DYANA calculation; Fig. 8S. RMS
10 fluctuation calculated for each residues of structures E and F.
11
12
13
14
15
16
17
18
19
20
21
22
23
24

25 References

- 26 1. J. Ghiso, A. Rostagno, Y. Tomidokoro, T. Lashley, M. Bojsen-Moller, H.
27 Braendgaard, G. Plant, J. Holton, R. Lal, T. Revesz, B. Frangione, *Brain Pathol*, 2006, **16**,
28 71-79.
- 29 2. R. Vidal, B. Frangione, A. Rostagno, S. Mead, T. Revesz, G. Plant, J. Ghiso, *Nature*,
30 1999, **399**, 776-781.
- 31 3. R. Vidal, T. Revesz, A. Rostagno, E. Kim, J. L. Holton, T. Bek, M. Bojsen-Moller, H.
32 Braendgaard, G. Plant, J. Ghiso, B. Frangione, *Proc. Natl. Acad. Sci. USA*, 2000, **97**, 4920-
33 4925.
- 34 4. D. P. Jones, *J. Intern. Med.*, 2010, **268**, 432-448.
- 35 5. D. P. Jones, Y. M. Go, *Diabetes Obes. Metab.*, 2010, **12**, 116-125.
- 36 6. T. E. Golde, *J. Clin. Invest.*, 2003, **111**, 11-18.
- 37 7. S. H. Kim, R. Wang, D. J. Gordon, J. Bass, D. F. Steiner, D. G. Lynn, G. Thinakaran,
38 S. C. Meredith, S. S. Sisodia, *Nat. Neurosci.*, 1999, **2**, 984-988.
- 39 8. S. I. Choi, R. Vidal, B. Frangione, E. Levy, *FASEB J.*, 2003, **17**, 373-375.
- 40 9. M. Tsachaki, J. Ghiso, A. Rostagno, S. Efthimiopoulos, *Neurobiol. Aging*, 2010, **31**,
41 88-98.
- 42 10. G. Gibson, N. Gunasekera, M. Lee, V. Lelyveld, O. M. A. El-Agnaf, A. Wright, B.
43 Austen, *J. Neurochem.*, 2004, **88**, 281-290.
- 44 11. O. M. A. El-Agnaf, J. M. Sheridan, C. Sidera, G. Siligardi, R. Hussain, P. I. Haris, B.
45 M. Austen, *Biochemistry*, 2001, **40**, 3449-3457.
- 46 12. O. M. A. El-Agnaf, S. Nagala, B. P. Patel, B. M. Austen, *J Mol Biol*, 2001, **310**, 157-
47 168.
- 48 13. J. Kim, V. M. Miller, Y. Levites, K. J. West, C. W. Zwizinski, B. D. Moore, F. J.
49 Troendle, M. Bann, C. Verbeeck, R. W. Price, L. Smithson, L. Sonoda, K. Wagg, V.
50 Rangachari, F. Zou, S. G. Younkin, N. Graff-Radford, D. Dickson, T. Rosenberry, T. E.
51 Golde, *J. Neurosci.*, 2008, **28**, 6030-6036.
- 52 14. T. Sato, P. Kienlen-Campard, M. Ahmed, W. Liu, H. L. Li, J. I. Elliott, S. Aimoto, S.
53 N. Constantinescu, J. N. Octave, S. O. Smith, *Biochemistry-U.S.*, 2006, **45**, 5503-5516.
54
55
56
57
58
59
60

15. W. Liu, E. Crocker, W. Y. Zhang, J. I. Elliott, B. Luy, H. L. Li, S. Aimoto, S. O. Smith, *Biochemistry-Us*, 2005, **44**, 3591-3597.
16. S. Matsuda, Y. Matsuda, E. L. Snapp, L. D'Adamio, *Neurobiol. Aging*, 2011, **32**, 1400-1408.
17. A. Binolfi, L. Quintanar, C. W. Bertocini, C. Griesinger, C. O. Fernandez, *Coordin. Chem. Rev.*, 2012, **256**, 2188-2201.
18. C. Hureau, *Coordin. Chem. Rev.*, 2012, **256**, 2164-2174.
19. C. Hureau, P. Dorlet, *Coordin. Chem. Rev.*, 2012, **256**, 2175-2187.
20. A. Khan, A. E. Ashcroft, O. V. Korchazhkina, C. Exley, *J. Inorg. Biochem.*, 2004, **98**, 2006-2010.
21. C. Migliorini, E. Porciatti, M. Luczkowski, D. Valensin, *Coord. Chem. Rev.*, 2012, **256**, 352-368.
22. Y. Miller, B. Y. Ma, R. Nussinov, *Coordin. Chem. Rev.*, 2012, **256**, 2245-2252.
23. S. Morante, *Curr. Alzh. Res.*, 2008, **5**, 508-524.
24. K. I. Silva, S. Saxena, *J. Phys. Chem. B*, 2013, **117**, 9386-9394.
25. F. Stellato, A. Spevacek, O. Proux, V. Minicozzi, G. Millhauser, S. Morante, *Eur. Biophys. J.*, 2011, **40**, 1259-1270.
26. J. H. Viles, *Coordin. Chem. Rev.*, 2012, **256**, 2271-2284.
27. I. Zawisza, M. Rozga, W. Bal, *Coordin. Chem. Rev.*, 2012, **256**, 2297-2307.
28. F. M. Zhou, G. L. Millhauser, *Coordin. Chem. Rev.*, 2012, **256**, 2285-2296.
29. R. De Ricco, S. Potocki, H. Kozlowski, D. Valensin, *Coord. Chem. Rev.*, 2014, **269**, 1-12.
30. A. Bharti, P. Bharati, M. K. Bharty, R. K. Dani, S. Singh, N. K. Singh, *Polyhedron*, 2013, **54**, 131-139.
31. F. Camponeschi, D. Valensin, I. Tessari, L. Bubacco, S. Dell'Acqua, L. Casella, E. Monzani, E. Gaggelli, G. Valensin, *Inorg. Chem.*, 2013, **52**, 1358-1367.
32. R. De Ricco, S. Potocki, H. Kozlowski, D. Valensin, *Coord. Chem. Rev.*, 2014, **269**, 1-12.
33. P. Faller, C. Hureau, P. Dorlet, P. Hellwig, Y. Coppel, F. Collin, B. Alies, *Coord. Chem. Rev.*, 2012, **256**, 2381-2396.
34. J. F. Jiang, I. A. Nadas, M. A. Kim, K. J. Franz, *Inorg. Chem.*, 2005, **44**, 9787-9794.
35. M. A. Kihlken, C. Singleton, N. E. Le Brun, *J. Biol. Inorg. Chem.*, 2008, **13**, 1011-1023.
36. B. O. Leung, F. Jalilehvand, V. Mah, M. Parvez, Q. Wu, *Inorg. Chem.*, 2013, **52**, 4593-4602.
37. M. Luczkowski, B. A. Zeider, A. V. H. Hinz, M. Stachura, S. Chakraborty, L. Hemmingsen, D. L. Huffman, V. L. Pecoraro, *Chem. Eur. J.*, 2013, **19**, 9042-9049.
38. O. Seneque, S. Crouzy, D. Boturnyn, P. Dumy, M. Ferrand, P. Delangle, *Chem. Commun.*, 2004, 770-771.
39. L. M. Utschig, T. Baynard, C. Strong, T. V. OHalloran, *Inorg. Chem.*, 1997, **36**, 2926-2927.
40. L. M. Utschig, J. G. Wright, G. Dieckmann, V. Pecoraro, T. V. Ohalloran, *Inorg. Chem.*, 1995, **34**, 2497-2498.
41. G. C. Vanstein, G. Vankoten, K. Vrieze, C. Brevard, A. L. Spek, *J. Am. Chem. Soc.*, 1984, **106**, 4486-4492.
42. W. C. Chan, P. D. White, *Fmoc solid phase peptide synthesis : a practical approach*. Oxford University Press: New York, 2000; p xxiv, 346 p.
43. H. M. Irving, M. G. Miles, L. D. Pettit, *Anal. Chim. Acta*, 1967, **38**, 475-488.
44. P. Gans, A. Sabatini, A. Vacca, *Talanta*, 1996, **43**, 1739-1753.
45. G. L. Ellman, *Arch. Biochem. Biophys.*, 1959, **82**, 70-77.

- 1
2
3 46. O. Iranzo, P. W. Thulstrup, S. B. Ryu, L. Hemmingsen, V. L. Pecoraro, *Chem. Eur. J.*,
4 2007, **13**, 9178-9190.
5 47. P. Guntert, C. Mumenthaler, K. Wuthrich, *J. Mol. Biol.*, 1997, **273**, 283-298.
6 48. D. Van der Spoel, E. Lindahl, B. Hess, G. Groenhof, A. E. Mark, H. J. C. Berendsen,
7 *J. Comput. Chem.*, 2005, **26**, 1701-1718.
8 49. W. R. P. Scott, P. H. Hunenberger, I. G. Tironi, A. E. Mark, S. R. Billeter, J. Fennen,
9 A. E. Torda, T. Huber, P. Kruger, W. F. van Gunsteren, *J. Phys. Chem. A*, 1999, **103**, 3596-
10 3607.
11 50. U. Essmann, L. Perera, M. L. Berkowitz, T. Darden, H. Lee, L. G. Pedersen, *J. Chem.*
12 *Phys.*, 1995, **103**, 8577-8593.
13 51. H. J. C. Berendsen, J. P. M. Postma, W. F. Vangunsteren, A. Dinola, J. R. Haak, *J.*
14 *Chem. Phys.*, 1984, **81**, 3684-3690.
15 52. T. Ban, D. Hamada, K. Hasegawa, H. Naiki, Y. Goto, *J. Biol. Chem.*, 2003, **278**,
16 16462-16465.
17 53. H. LeVine, *Arch. Biochem. Biophys.*, 1997, **342**, 306-316.
18 54. V. N. Uversky, S. Longhi, *Instrumental analysis of intrinsically disordered proteins :
19 assessing structure and conformation*. Wiley: Hoboken, N.J., 2010; p xxix, 744 p., 716 p. of
20 plates.
21 55. W. Stricks, I. M. Kolthoff, *J. Am. Chem. Soc.*, 1953, **75**, 5673-5681.
22 56. R. Strand, W. Lund, J. Aaseth, *J. Inorg. Biochem.*, 1983, **19**, 301-309.
23 57. S. Pires, J. Habjanic, M. Sezer, C. M. Soares, L. Hemmingsen, O. Iranzo, *Inorg.*
24 *Chem.*, 2012, **51**, 11339-11348.
25 58. H. Kozłowski, W. Bal, M. Dyba, T. Kowalik-Jankowska, *Coord. Chem. Rev.*, 1999,
26 **184**, 319-346.
27 59. T. Kowalik-Jankowska, M. Ruta-Dolejsz, K. Wisniewska, L. Lankiewicz, *J. Inorg.*
28 *Biochem.*, 2002, **92**, 1-10.
29 60. D. Witkowska, S. Bielinska, W. Kamysz, H. Kozłowski, *J. Inorg. Biochem.*, 2011,
30 **105**, 208-214.
31 61. P. Giannozzi, K. Jansen, G. La Penna, V. Minicozzi, S. Morante, G. Rossi, F. Stellato,
32 *Metallomics*, 2012, **4**, 156-165.
33 62. F. Guerrieri, V. Minicozzi, S. Morante, G. Rossi, S. Furlan, G. La Penna, *J. Biol.*
34 *Inorg. Chem.*, 2009, **14**, 361-374.
35 63. C. Migliorini, A. Sinicropi, H. Kozłowski, M. Luczkowski, D. Valensin, *J. Biol.*
36 *Inorg. Chem.*, 2014, **19**, 635-645.
37 64. L. Quintanar, L. Rivillas-Acevedo, R. Grande-Aztatzi, C. Z. Gomez-Castro, T. Arcos-
38 Lopez, A. Vela, *Coord. Chem. Rev.*, 2013, **257**, 429-444.
39 65. T. M. DeSilva, G. Veglia, F. Porcelli, A. M. Prantner, S. J. Opella, *Biopolymers*, 2002,
40 **64**, 189-197.
41 66. P. Rousselot-Pailley, O. Seneque, C. Lebrun, S. Crouzy, D. Boturyn, P. Dumy, M.
42 Ferrand, P. Delangle, *Inorg. Chem.*, 2006, **45**, 5510-5520.
43 67. R. Srinivasan, E. M. Jones, K. Liu, J. Ghiso, R. E. Marchant, M. G. Zagorski, *J. Mol.*
44 *Biol.*, 2003, **333**, 1003-1023.
45
46
47
48
49
50
51
52
53
54
55
56
57
58
59
60